Andrea Belleri. 2017. "Displacement based design for precast concrete frames with not-emulative connections". Engineering Structures, Vol. 141, pp. 228-240. DOI:10.1016/j.engstruct.2017.03.020

Publisher's version:
http://dx.doi.org/10.1016/j.engstruct.2017.03.020

Displacement based design for precast concrete frames with not-emulative connections

Andrea Belleri[1]
Department of Engineering and Applied Sciences, University of Bergamo, Italy

Abstract

The Displacement Based Design (DBD) methodology to precast concrete frame structures with not-emulative connections is investigated herein. The seismic design procedure is applied to both single-storey and multi-storey structures. Industrial and office buildings, warehouses and commercial malls with a structural layout typical of the European market are considered: cantilever columns resting on isolated footings connected at the floor level to pre-stressed precast beams, supporting pre-stressed precast concrete floor or roof elements. The need to control the lateral seismic displacement is dictated by the high flexibility of these structures, which in turn is associated to the structural scheme and to the inter-storey height.
Starting from the general displacement based design procedure, the paper focuses on how properly taking into account the influence of column-foundation and beam-column precast connections; expressions and procedures are developed to determine the yield curvature, the equivalent viscous damping, the effective height and the effective mass of the single degree of freedom substitute structure adopted in the DBD procedure.
The proposed procedure is applied to selected case studies and validated through non-linear time history analyses, showing the ability of the design procedure in controlling lateral displacements.

Keywords:
precast structures; seismic design; displacement based design; not-emulative connections; grouted sleeves connections; yield deflected shape; equivalent viscous damping;

1. Introduction

Precast concrete structures are widely adopted, especially in the industrial and commercial sector, due to the reduced on-site construction time and cost effectiveness, to the ability of covering wide spans with pre-stressed elements and to a better quality control of materials and structural elements compared to traditional reinforced concrete structures. Although different typologies of lateral force resisting system solutions are available in the literature and in the worldwide practice, such as reinforced concrete emulative structures [1, 2], jointed ductile connections [3-5] and rocking and hybrid walls [6, 7] among others, the majority of European industrial buildings, warehouses and commercial malls are single-storey or few-storey buildings with a simple structural layout: cantilever columns, connected at the floor and at the roof by simply supported precast and pre-

[1] Assistant professor, Ph.D.; andrea.belleri@unibg.it

stressed beams, supporting pre-stressed concrete elements. The columns are placed and grouted on-site in isolated precast cup-footings or connected to shallow foundations through mechanical splices or grouted sleeve solutions [8-11]. The column-to-beam connection is typically pinned [12-14] and the energy dissipation is provided by the development of plastic hinges at the base of the columns.

The hinged-frame static scheme and the high inter-storey height lead to flexible structures in which the contribution of elastic displacements is higher compared to traditional reinforced concrete frames. If not appropriately considered in the design phase, this high flexibility could lead to displacement incompatibility between structural elements [15, 16]; the contact between the end of the beam and the column during their relative rotations may lead to a change in the boundary conditions, and between structural and non-structural elements, such as precast cladding panels, causing their premature failure [17-23]. The seismic performance of these structures is therefore related to inter-storey drift control rather than material strain limitations.

The seismic design approach commonly adopted by professional engineers, as in EN 1998-1 [24], is the well known force based design (FBD): the equivalent lateral inertia forces are obtained considering a system with reduced flexural stiffness (an effective modulus of inertia I_{eff} is defined as a percentage of the gross module I_g to account for concrete cracking) and an acceleration spectrum scaled by a force reduction factor depending on the structural typology is used. The lateral displacements are obtained at the end of the design process. For flexible structures, as those considered herein, the displacements are obtained from the equal displacement approximation which states that the displacement ductility is equal to the force reduction factor.

Following the FBD procedure [25], the results could be affected by the aforementioned sources of approximations: the force reduction factor, the effective modulus of inertia and the equal displacement approximation. Although these limitations could be overcome by the definition of refined formulations, the displacements are evaluated at the end of the design process. Being lateral displacements so important in the seismic response of the structures considered herein, a more rational approach would consider the displacements as the input of the design process. Performance based design methodologies, such as displacement based design (DBD), follow this approach.

Starting from the DBD procedure proposed by Priestley et al. [26], the paper considers how to implement typical details of precast concrete structures, such as column-to-foundation and beam-to-column connections, in the design process. Regarding the column-to-foundation connections, the influence on the system energy dissipation capacity and on the yield curvature is investigated; the former affects the equivalent viscous damping formulation, while the latter affects the displacement ductility formulation. Regarding the beam-to-column connections, the paper analyzes the influence on the effective height and effective mass of the substitute structure used in the design process. Finally, the proposed procedure is applied to selected case studies, both single and multi-storey buildings, and validated by means of non linear time history analyses.

2. Displacement Based Design

The DBD procedure [26] adopts a substitute structure approach [27], which considers a single degree of freedom (SDOF) elastic structure with stiffness equal to the secant stiffness at maximum displacement and with damping equal to an equivalent viscous damping accounting for hysteretic energy dissipation.

The definition of the structural deflected shape (Δ_i) for a considered multi degrees of freedom (MDOF) system is the first step of the procedure. The deflected shape represents the first inelastic

mode of vibration and it is associated to a particular structural typology. Priestley et al. [26] report the deflected shapes for typical structural typologies, based on analytical derivations or as results of non-linear time history analyses. It is worth noting that the diaphragm stiffness could alter the lateral deflection, with greater lateral displacements in the central part of the diaphragm, especially when the lateral force resisting system is located at the diaphragm edges. The properties of the SDOF substitute structure, as the target displacement (Δ_d), the effective height (h_{eff}) and the effective mass (m_{eff}), are obtained directly from the MDOF-system target deflected shape, which is selected to limit, for instance, inter-storey drifts or material strains. Such properties are:

$$\Delta_d = \frac{\sum_{i=1}^{n} m_i \Delta_i^2}{\sum_{i=1}^{n} m_i \Delta_i}; \quad h_{eff} = \frac{\sum_{i=1}^{n} m_i \Delta_i h_i}{\sum_{i=1}^{n} m_i \Delta_i}; \quad m_{eff} = \frac{\sum_{i=1}^{n} m_i \Delta_i}{\Delta_d} \qquad (1)\ (2)\ (3)$$

The following step is the evaluation of the equivalent viscous damping, which accounts for the elastic (ξ_{el}) and the hysteretic (ξ_{hy}) damping: ξ_{el} considers material viscous damping, radiation damping due to the foundation system and damping due to non-structural components; ξ_{hy} considers the energy dissipation capacity of the system and depends on the hysteretic behaviour of the structural elements. Various equivalent viscous damping formulations are available in the literature [26, 28, 29]. The formulation adopted herein [29] depends on the effective period and displacement ductility of the SDOF substitute structure, being the displacement ductility represented by the ratio between design and yield displacement ($\mu_\Delta = \Delta_d / \Delta_y$):

$$\xi_{eq} = \xi_{el} + \xi_{hy} = 0.05 + a\left(1 - \frac{1}{\mu_\Delta^{\,b}}\right)\left(1 + \frac{1}{\left(T_{eff} + c\right)^d}\right) \qquad (4)$$

The parameters (*a, b, c, d*) depend on the non-linear properties (i.e. hysteretic model) of the structural elements and they are obtained by regression analysis. It is worth noting that, being T_{eff} not available at the beginning of the design process, a first tentative value is necessary, for instance T_{eff} = 1s, and subsequently updated. The hysteretic model considered as a reference herein is the Takeda model [30] whose force-displacement relationship (**Figure 1**) is defined by $\alpha = 0.3$, $\beta = 0.6$, $r = 0.05$; the corresponding parameters of Eqn. 4 are: $a = 0.249$, $b = 0.527$, $c = 0.761$ and $d = 3.250$.

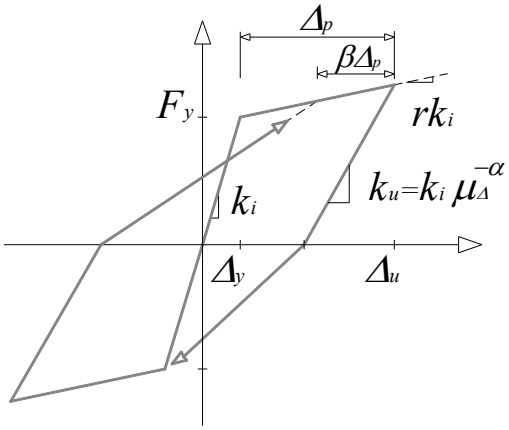

Figure 1 – Takeda hysteretic model.

The yield displacement (Δ_y) corresponds, for single-storey hinged frames, to a linear variation of the curvature from 0 to yield (ϕ_y), from the column tip to the column base; for multi storey structures, a

specific formulation of Δ_y will be defined in the following. According to Priestley et al. [26], the yield curvature of rectangular reinforced concrete elements can be related to the properties of the cross-section:

$$\Delta_y = \phi_y \times \frac{H^2}{3} = 2.1 \frac{\varepsilon_y}{B} \times \frac{H^2}{3} \tag{5}$$

B and H are the cross-section depth and the column height respectively; ε_y is the yield deformation of the longitudinal reinforcement.

The equivalent viscous damping is used to scale the elastic displacement spectrum (S_{D_el}) for damping values different from 5%. According to EN 1998-1 [24], this reduction is:

$$\eta = \frac{S_{D\_el}(\xi_{eq})}{S_{D\_el}(\xi_{eq} = 0.05)} = \sqrt{\frac{0.10}{0.05 + \xi_{eq}}} \tag{6}$$

The substitute structure effective period (T_{eff}) is the period of the damped displacement spectrum ($S_{D\_el}(\xi_{eq})$) corresponding to the target displacement (Δ_d). From T_{eff} it is possible to evaluate the effective stiffness (k_{eff}), associated to the substitute structure maximum response, and thereafter the design base shear (V_b):

$$V_b = k_{eff} \Delta_d = 4\pi^2 \frac{m_{eff}}{T_{eff}^2} \Delta_d \tag{7}$$

The obtained base shear is distributed as design forces along the height of the MDOF system considering the inelastic deflected shape:

$$F_i = \left(V_b m_i \Delta_i\right) / \left(\sum_{i=1}^{n} m_i \Delta_i \right) \tag{8}$$

Finally, capacity design principles are applied to inhibit fragile mechanisms.

It is worth noting that both Eqn. 4 parameters and the coefficients in Eqn. 6 depend on the ground motion set considered, i.e. the calibration of such equations leads to different parameters and coefficients if different ground motion sets are used; however, Pennucci et al. [31] showed that the resulting value of η (Eqn. 6) is not dependent on the ground motions set considered, providing that the same ground motion set is used in the calibration of both equations.

3. Column-to-foundation connections

The column-to-foundation connections used in precast structures influence the DBD procedure. In particular, they affect the yield curvature and the energy dissipation capacity of the structural system. Typical connections are represented by cup footings, mechanical splices and grouted sleeve solutions.

3.1 Yield curvature

As reported in Eqn. 5, the yield curvature (ϕ_y) affects directly the yield displacement (Δ_y); as a result, the equivalent viscous damping is also affected, being dependent on the displacement ductility. The yield curvature formulation of Eqn. 5 was obtained [26] analysing square columns with a cross-section size equal to 160 cm, a concrete cover equal to 5 cm and longitudinal re-bars equally distributed along the section sides. This equation does not properly describe the yield curvature when the effective depth is not as close to the cross-section size, as in the case of grouted

sleeve solutions [9]. To overcome this limitation, the cross-section size B is substituted with the cross-section effective depth d_s, and the constant 2.1 with the parameter α_1:

$$\phi_y = \alpha_1 \cdot \frac{\varepsilon_y}{d_s} \tag{9}$$

α_1 is obtained by a least square procedure on the results of moment-curvature analyses conducted with the computer code Cumbia [32], accounting for the influence of different variables such as the cross-section size (A_c), the concrete cover (c_c), the concrete compressive strength (f_c), the steel yield strength (f_y), the steel overstrength ratio (ratio between ultimate f_u and yield stress), the axial load ratio ($\nu = N/A_c f_{ck}$, where N is the axial load) and the ratio (ρ) between the longitudinal reinforcement area and A_c. Four different sets of longitudinal reinforcement were evaluated: 4, 8, 12 and 16 re-bars equally spaced along the cross-section's sides. A sensitivity analysis has been conducted to check the influence of the selected variables; the results are reported in **Table 1** in terms of the maximum recorded scatter to the reference case (A_c = 45x45 cm, c_c = 5 cm; f_c = 40 MPa; f_y = 500 MPa; f_u/f_y = 1.3; ρ = 0.02; ν = 0.15).

Table 1. Results of the sensitivity analysis

Variable	Range	Max. difference (%)
A_c	900 – 3600 cm^2	3.1%
c_c	3 – 8 cm	3.7%
f_c	30 – 60 MPa	4.2%
f_y	450 – 550 MPa	3.1%
f_u/f_y	1.1 – 1.5	0%
ρ	0.005 – 0.04	21.0%
ν	0.05 – 0.30	15.6%

Among these parameters, ν and ρ have been selected to describe α_1:

$$\alpha_1 = \frac{\phi_y \cdot d_s}{\varepsilon_y} = h_1 \cdot \nu + h_2 \cdot \rho + h_3 \tag{10}$$

Table 2 shows the values of h_1, h_2 and h_3 as a function of the total number of longitudinal re-bars.

Table 2. Yield curvature coefficients

Parameter	Number of longitudinal rebars			
	4	8	12	16
h_1	1.94	1.11	1.22	1.97
h_2	9.18	6.50	6.30	4.30
h_3	1.39	1.69	1.69	1.18

3.2 Energy dissipation capacity

The use of different column-to-foundation connections is generally associated to different hysteretic models and to different plastic hinge lengths; as, for instance, the strain penetration associated to various mechanical connectors used in precast buildings leads to differences in the plastic hinge length. The difference in the energy dissipation capacity is directly related to the equivalent viscous damping adopted in the DBD procedure.

A procedure is herein proposed in order to calibrate the hysteretic damping expression associated to various types of column-to-base connections. The procedure represents an alternative to [29] and it is based on the analysis of the force displacement inelastic response of SDOF systems. The procedure is summarized in the following steps and graphically represented in **Figure 2**.

1. Select the hysteretic model whose hysteretic damping needs to be calibrated. In this case the chosen hysteretic model is the most representative of the force-displacement relationship of the considered column-to-foundation subassembly.
2. Select a displacement ductility value (μ_Δ).
3. Get the elastic spectral displacement ($S_{D\_el}(T)$) and the constant ductility inelastic spectral displacement ($S_{D\_in}(T,\mu_\Delta)$); the latter could be obtained by finite element software or by dedicated tools, such as Ruaumoko-Inspect [33].
   It is important to note that the inelastic spectral displacement refers to a SDOF systems with a given elastic period (T_0), while the hysteretic damping equation (Eqn. 4) includes the effective period (T_{eff}). The relationship between T_0 and T_{eff}, for hysteretic systems with a backbone loading curve resembling a bilinear curve with post-yield stiffness ratio r, is:
   $$T_0 = T_{eff}\sqrt{\frac{1+r(\mu_\Delta-1)}{\mu_\Delta}} \tag{11}$$
   Therefore, in order to allow the comparison between $S_{D\_el}(T)$ and $S_{D\_in}(T,\mu_\Delta)$, it is required to consider the elastic spectral displacement of the substitute system ($S_{D\_el}(T_{eff})$), with $T=T_{eff}$, and the inelastic spectral displacement of the initial SDOF system ($S_{D\_in}(T_0,\mu_\Delta)$), with $T=T_0$.
4. Select an effective period T_{eff} and determine the corresponding T_0 from Eqn. 11.
5. Evaluate $S_{D\_el}(T_{eff})$ and $S_{D\_in}(T_0,\mu_\Delta)$ from the displacement spectra previously obtained.
6. Determine the hysteretic damping directly from Eqn. 6, where $S_{D\_el}(\xi_{eq})$ and $S_{D\_el}(5\%)$ are substituted with $S_{D\_in}(T_0,\mu_\Delta)$ and $S_{D\_el}(T_{eff})$ respectively.
   $$\xi_{hyst}\left(T_{eff},\mu_\Delta\right)=\xi_{eq}\left(T_{eff},\mu_\Delta\right)-0.05=$$
   $$=\left(0.10\cdot\left(\frac{S_{D\_el}(T_{eff})}{S_{D\_in}(T_0)}\right)^2-0.05\right)-0.05=0.10\cdot\left[\left(\frac{S_{D\_el}(T_{eff})}{S_{D\_in}(T_0)}\right)^2-1\right] \tag{12}$$
7. The equivalent viscous damping equation parameters are obtained by means of a least square regression, based on the average value (or a selected percentile) of the ground motion inelastic spectra.
8. Repeat for different T_{eff}.
9. Repeat for different μ_Δ.

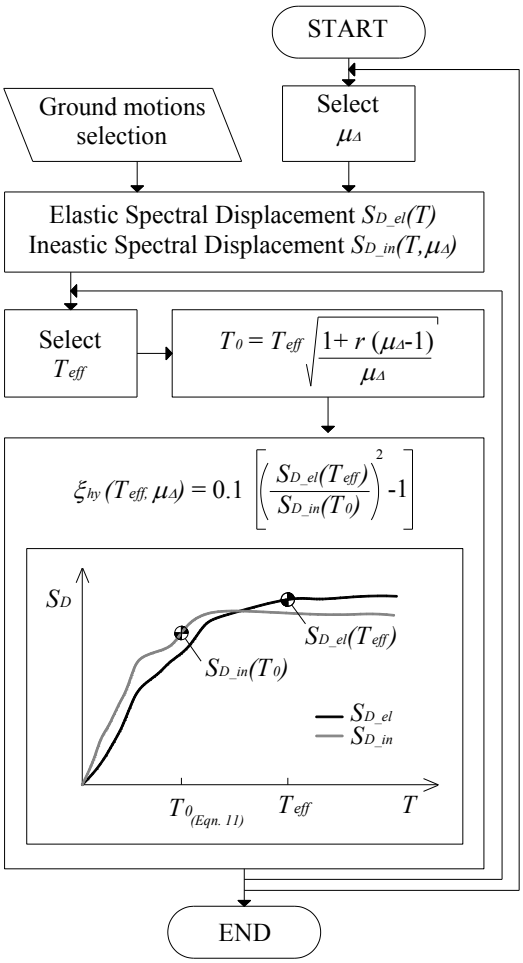

198

199 **Figure 2** – Flow chart for the hysteretic damping calibration

200 The proposed procedure is applied to the unbonded grouted sleeves connection (**Figure 3**) reported
201 in Belleri and Riva [11]. The Takeda parameters governing the hysteretic response of the reported
202 experimental test are r = 0.005, α = 0.35 and β = 0. Given the hysteretic response parameters, the
203 proposed calibration procedure has been applied. The obtained Eqn. 4 parameters are a = 2.356,
204 b = 0.027, c = 0.634 and d = 0.703, suitable for effective periods in the range (0.5s-4s) and
205 displacement ductility in the range (1-4). A conservative equivalent viscous damping estimation,
206 independent from the effective period, has been also derived:

207 $$\xi_{eq} = \xi_{el} + \xi_{hy} = 0.05 + 0.39\left(1 - \frac{1}{\mu_\Delta^{0.25}}\right) \quad (13)$$

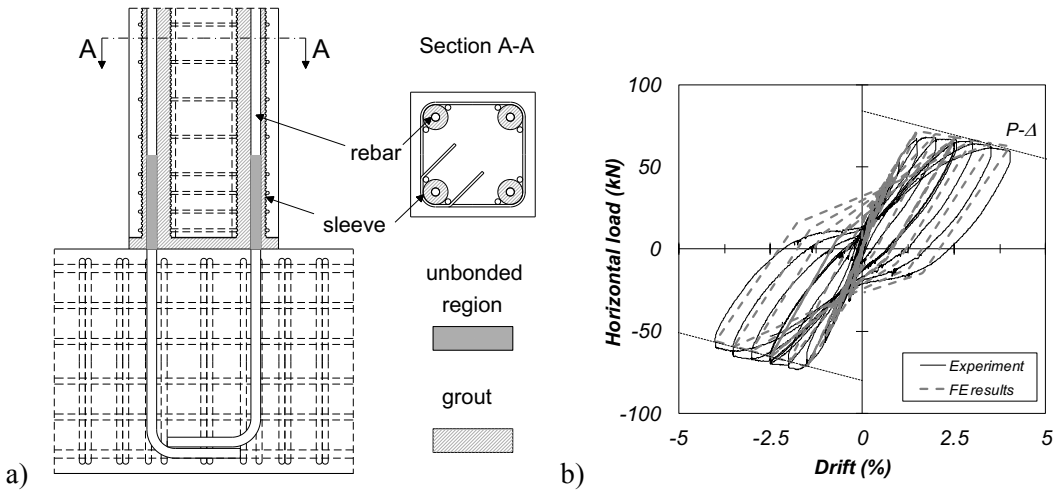

Figure 3 – Unbonded grouted sleeve solution:
a) typical details; b) experiment versus FE comparison.

4. Beam-to-column connections

Considering EN 1998–1 [24], precast connections are classified based on their position compared to the energy dissipation regions of the structure: (i) connections outside critical regions; (ii) connections inside critical regions but overdesigned to remain elastic and (iii) connections inside critical regions with adequate ductility and dissipation capacity. For precast frames with beam-to-column hinged connections, the energy dissipation is provided by the development of a plastic hinge at the base of the column; in this case the beam-to-column connections are identified as type (i) and designed as pinned connections.
The effect of beam-to-column connections other than pinned is considered herein, distinguishing between single-storey and multi-storey frames.

4.1 Single-storey frames

In the case of single-storey frames, a SDOF substitute structure with appropriate effective mass and height is defined. A representative scheme is depicted in **Figure 4** for lateral and central columns. Considering beam-to-column and column-to-foundation connections with a bilinear hysteretic model (elasto-plastic, Takeda or others), the first inelastic mode shape is assumed as a rigid base rotation of the structure after yielding of such connections. In fact, after this condition, a mechanism develops. The considered structure is reduced by static condensation to a SDOF system.

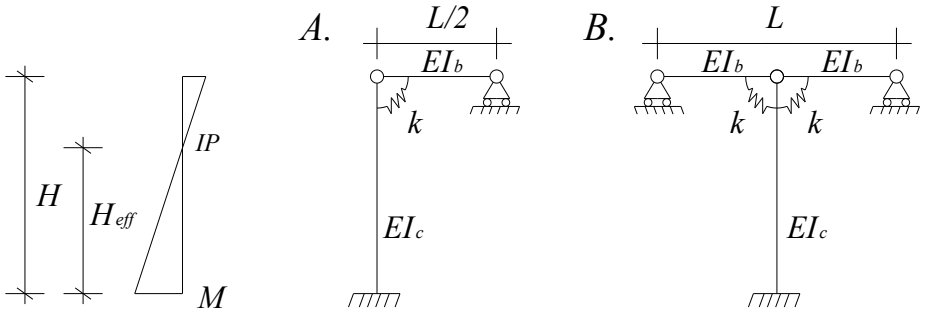

Figure 4 – Beam-to-column representative scheme.
Note: EI_b and EI_c are the beam and column flexural stiffness, respectively; k connection stiffness; L and H are the beam and column length, respectively; H_{eff} is the effective height and IP is the inflection point.

Assuming that both the beam-to-column and column-to-foundation connections have yielded, the roof yield displacement is obtained from double integration of the column curvature according to the moment distribution in **Figure 4**, considering a bending moment at the column tip equal to M_y^{con} and $2M_y^{con}$ for configurations A and B, respectively:

$$\Delta_{y\ A}^{roof} = \left(\phi_y^{col} - \frac{M_y^{con}}{2EI_c}\right)\frac{H^2}{3}; \quad \Delta_{y\ B}^{roof} = \left(\phi_y^{col} - \frac{M_y^{con}}{EI_c}\right)\frac{H^2}{3} \tag{14) (15}$$

where ϕ_y^{col} is the column curvature at yield, M_y^{con} is the yield moment of the beam-to-column connection, EI_c is the column flexural stiffness.

The resulting substitute structure is characterized by an effective mass (m_{eff}) equal to the whole roof mass, being the original system reduced to a SDOF by static condensation, and an effective height (H_{eff}) corresponding to the column inflection point (IP in **Figure 4**). The target displacement is associated to a target inter-storey drift (β), as typically governing the considered precast concrete structures. Referring to configuration B (**Figure 4**), the plastic roof displacement, defined as the roof displacement associated to the rotation of the plastic hinge at the column base, is obtained by subtracting the roof yield displacement (Eqn. 15) to the target displacement:

$$\Delta_{plast}^{roof} = \Delta_{\text{target}}^{roof} - \Delta_y^{roof} = \beta H - \phi_y^{col}\frac{H^2}{3}\left(1-\alpha_2\right) \tag{16}$$

where α_2 is the ratio between the yield moment of the beam-to-column (M_y^{con}) and column-to-foundation (M_y^{col}) connection. For sake of clarity, it is worth noting that α_2 refers to the value of a single beam-to-column connection of configuration B (M_y^{con}) and not to the bending moment at the top of the column ($2M_y^{con}$). Therefore, the substitute structure target displacement, evaluated at a height equal to the column inflection point, is:

$$\Delta_d^{IP} = \Delta_y^{IP} + \Delta_{plast}^{IP} = \frac{\phi_y^{col}H^2}{3}\frac{\alpha_2\left(2\alpha_2-1\right)}{\left(1+2\alpha_2\right)^2} + \frac{\beta H}{1+2\alpha_2} \tag{17}$$

The associated displacement ductility is:

$$\mu_\Delta = \frac{\Delta_d^{IP}}{\Delta_y^{IP}} = \alpha_2\left(2\alpha_2-1\right) + \frac{3\beta\left(1+2\alpha_2\right)}{\phi_y^{col}H} \tag{18}$$

The derivation of Eqn. 17 and 18 is reported in Appendix A. Based on these data, it is possible to apply the DBD procedure shown before.

As already mentioned, the previous formulas have been derived for central columns, configuration B in **Figure 4**. In the case of portal frames or perimeter columns, configuration A in **Figure 4**, α_2 needs to be substituted by $0.5\alpha_2$ in the previous equations. For multiple bays it is herein considered the weighted value:

$$\alpha_{2,weighted} = \alpha_2 \frac{0.5 \cdot n_{per\ col} + n_{int\ col}}{n_{per\ col} + n_{int\ col}} \tag{19}$$

where $n_{per\ col}$ and $n_{int\ col}$ is the number of perimeter and interior columns, respectively.

The resulting DBD procedure needs iterations, being α_2 unknown at the beginning. In order to get a first estimation of α_2, it is suggested to apply the DBD procedure neglecting the beam-to-column connection contribution, i.e. $M_y^{con} = 0$ and $\alpha_2 = 0$, then evaluate α_2 at the end of the DBD procedure and iterate. It is worth noting that the presence of beam-to-column connections is associated to a shear load (V_i) at each beam end which modifies the axial load in the columns; this contributes to resist the total overturning moment as highlighted in **Figure 5c** for multi-storey frames. Therefore, the total overturning moment due to the lateral seismic loads is counteracted by the bending moment developed at the columns base (M_{bi}) and the overturning moment associated to such axial load ($T \cdot L_{tot}$, in the case of equal connections and equal spans). In order to estimate the design moment at the column bases, the contribution of the overturning moment $T \cdot L_{tot}$ is to be detracted from the total overturning moment obtained following the DBD approach.

4.2 Multi-storey frames

In the case of multi-storey frames, three situations are identified based on the beam-to-column connections (**Figure 5**). **Figure 5a** and **5b** show similar hinged connections differing from each other by the gap at the beam-to-column interface, which results in different connection rotation capacity before the contact between the column and the beam. **Figure 5a** represents a connection able to ensure the rotation compatibility between the connected elements, being the rotation demand concentrated at the joint region due to its lower stiffness compared to the connected precast concrete elements. The static scheme is therefore a hinged-frame. **Figure 5b** shows a connection with different behaviours in the clockwise and counter-clockwise rotations: in the former, the connection is actually a hinge; in the latter, the free rotation is available until closure of the gap between the two structural elements, then the sub-assemblage gains rotational stiffness. The resulting static scheme depends on the direction of the lateral loads and it is represented by a hinge connection at one beam end and by a degree of fixity at the other end. **Figure 5c** considers a connection specifically designed to provide a rotational degree of fixity and to dissipate seismic energy; this type of connection involves mechanical devices, such as buckling inhibited bars [34], and it is compatible with precast pre-stressed elements being dry installed after the floor erection. The resulting static scheme is represented by a degree of fixity at both beam ends. As mentioned before for single-storey frames, a shear load (V_i) develops at each beam end (**Figure 5b,c**) as a consequence of beam-to-column connections which modifies the axial load in the columns. In the case of equal connections and equal spans, as represented in **Figure 5** and considered herein, only the axial load of the lateral columns is affected by V_i; in fact the sum of V_i at each side of the inner columns is zero. This contributes to resist the total overturning moment by an amount equal to $T \cdot L_{tot}$. Therefore, in order to estimate the design moment at the column base (M_{bi}), the contribution

of the overturning moment $T{\cdot}L_{tot}$ is to be detracted from the total overturning moment obtained following the DBD approach.

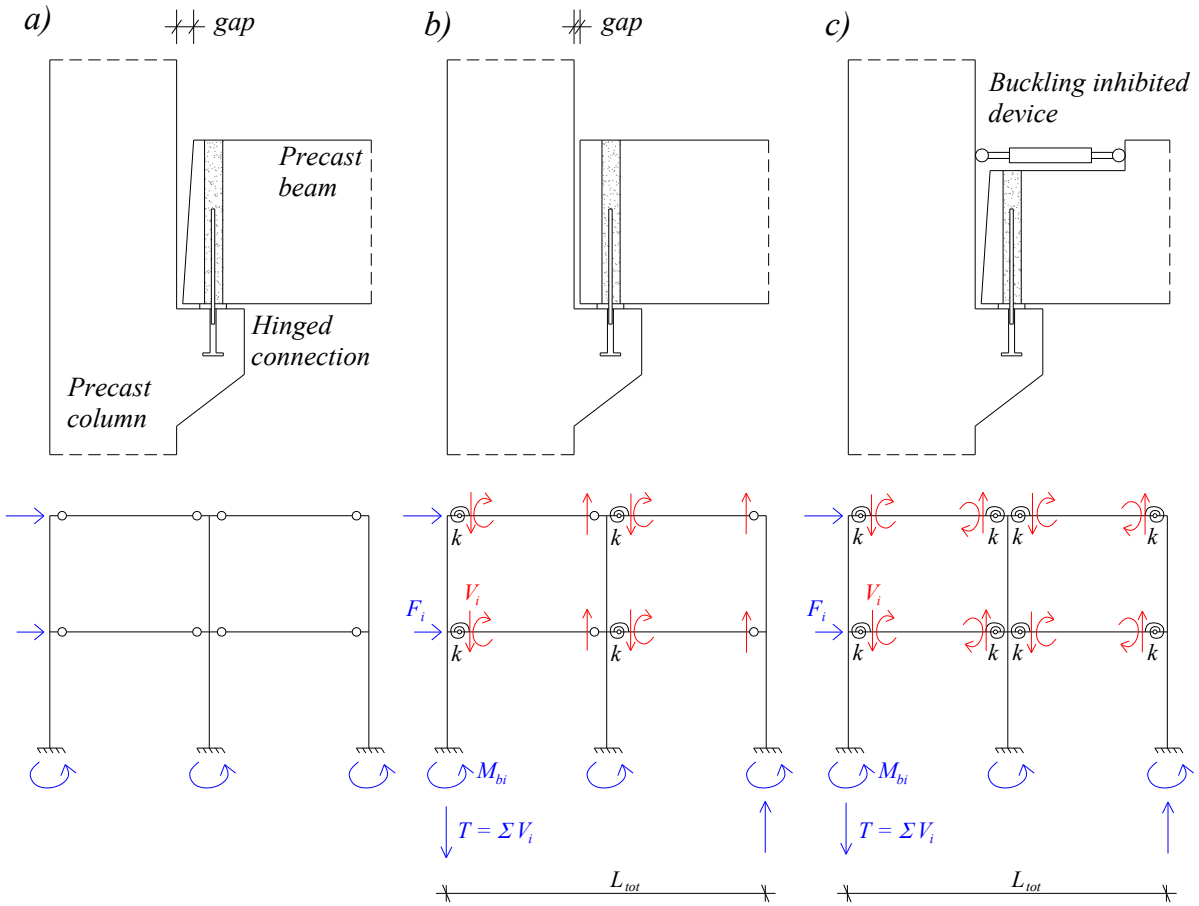

Figure 5 – Beam-to-column connections and resulting static schemes

An important aspect of the DBD procedure is the definition of the inelastic deflected shape. In the case of hinged-frames, the available formula [26] for shear walls could be applied, considering the column yield curvature expression proposed herein (Eqn. 10):

$$\Delta_{y,i} = \phi_y \frac{H_i^2}{2}\left(1-\frac{H_i}{3H_n}\right) = \alpha_1 \cdot \frac{\varepsilon_y}{d_s}\frac{H_i^2}{2}\left(1-\frac{H_i}{3H_n}\right) \tag{20}$$

Where H_i and H_n are the height of the ith and roof level respectively. The formula is obtained from a triangular distribution of bending moment along the column height. Considering instead a triangular distribution of lateral forces at each floor and applying the fundamental properties of series, the yield displacement at the ith floor is (derivation reported in Appendix B):

$$\Delta_{y,i}^{hinged} = \frac{\phi_y}{2n^2+3n+1}\left[\frac{H_i^5}{20\cdot H_n^3}n^2 - \frac{H_i^3}{6\cdot H_n}\left(3n^2+3n+1\right)+\frac{H_i^2}{2}\left(2n^2+3n+1\right)\right] \tag{21}$$

It is worth noting that Eqn. 21 becomes the formula presented in [35] for n, total number of floors, tending to infinite and it is valid also for shear walls.

In the case of partially fixed beam-to-column connections, the yield deflected shape becomes (derivation reported in Appendix C):

$$\Delta_{y,i}^{connection} = \Delta_{y,i}^{hinged}\left(1+n\cdot\alpha_3\right) - \frac{\alpha_3}{2}\phi_y\left[-\frac{n\cdot H_i^3}{3\cdot H_n}+\left(n+\frac{1}{2}\right)H_i^2 - \frac{H_i\cdot H_n}{6\cdot n}\right] \tag{22}$$

where α_3 is equal to α_2 for the static scheme of **Figure 5b** and the lateral columns of **Figure 5c**, and equal to twice α_2 for the interior columns of **Figure 5c**, being α_2 the ratio between the yield moment of beam-to-column and column-to-foundation connection as mentioned before. A weighted value of α_3 could be considered for the static scheme depicted in **Figure 5c** similarly to Eqn. 19. Eqn. 22 is also suitable for coupled shear walls. The rotations at the connection level are obtained deriving Eqn 20-22 with respect to H_i (Appendix C). Post yield displacements are obtained from Eqn 20-22 by adding the displacements associated to the plastic hinge rotation at the column base.

4.3 Equivalent viscous damping

For both cases, single-storey and multi-storey frames, it is possible to evaluate the substitute structure equivalent viscous damping [26] by a weighted average of the hysteretic damping associated to the columns and connections, in which the weights are the respective dissipated energies ($E_{diss\ col}$, $E_{diss\ con}$):

$$\xi_{eq} = \xi_{el} + \frac{\xi_{hy\ col} \cdot E_{diss\ col} + \xi_{hy\ con} \cdot E_{diss\ con}}{E_{diss\ col} + E_{diss\ con}} \tag{23}$$

To evaluate the dissipated energy at the column base, according to Takeda hysteresis, it is possible to consider the following approximated formulas, valid respectively for Takeda parameters $\alpha = 0.3$ $\beta = 0.6$ $r = 0.05$, as in [29], and $\alpha = 0.35$ $\beta = 0$ $r = 0.005$, as for the grouted sleeve solution mentioned before:

$$E_{diss\ col} = \left[6 - 0.1\mu_\Delta - 6\mu_\Delta^{-0.7}\right] \cdot E_{el\ col}; \quad E_{diss\ col} = 4\left[1 - \mu_\Delta^{-0.65}\right] \cdot E_{el\ col} \tag{24, 25}$$

$E_{el\ col}$ is the half product of the maximum column bending moment times the maximum base rotation.

The dissipated energy at the beam-to-column connection depends on the actual hysteresis, which varies based on the inelastic mechanism. In the case of unknown hysteresis, it is suggested to neglect the connection contribution in the substitute structure equivalent viscous damping.

5. DBD procedure application to selected case studies

Two case studies are considered representing single-storey and multi-storey precast buildings. A scheme of the finite element models is shown in **Figure 6**. In both cases, the concrete 28-day cylindrical strength and the steel reinforcement yield stress are assumed equal to 40 MPa and 450 MPa, respectively. Non-linear time history (NLTH) analyses are conducted [36] considering a set of seven ground motions[2] selected and scaled from the European strong motion database [37] in order to be spectrum compatible with EN 1998–1 [24] type 1 spectrum, soil type C, and peak ground acceleration on rock equal to 0.30 g.

[2] Record code [37] and scale factor in brackets: 000333xa (1.75), 000333ya (1.68), 001726xa (1.83), 001726ya (1.49), 000133xa (3.70), 000335ya (3.36), 000348ya (12.93)

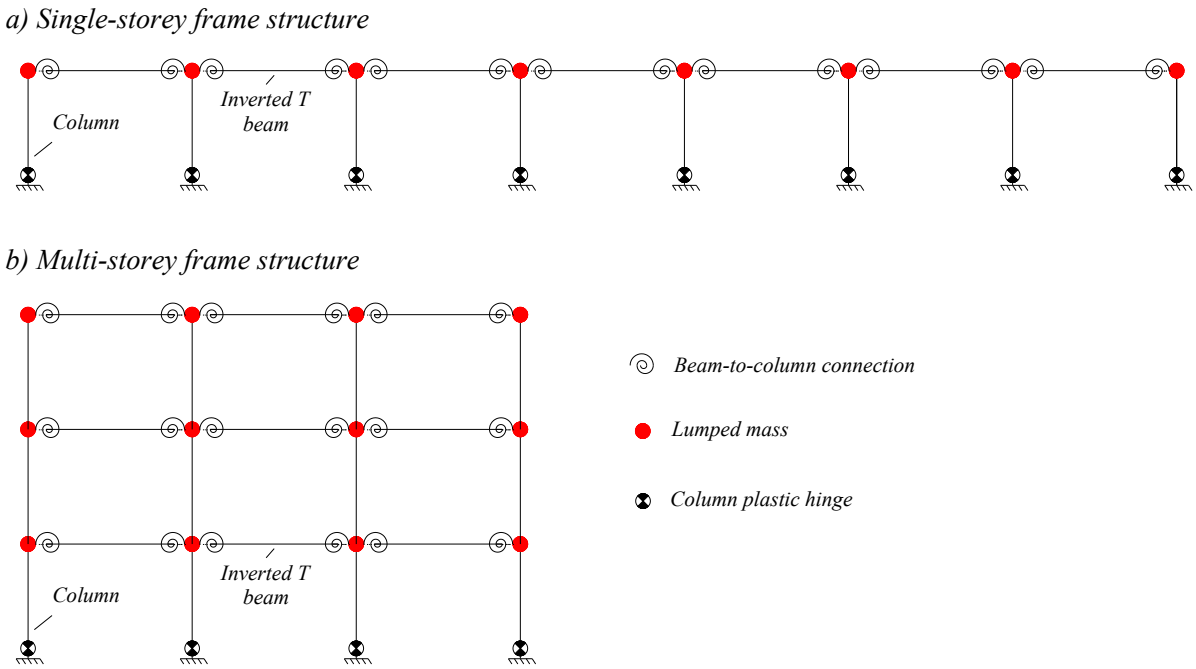

Figure 6 – Finite element scheme: a) single-storey and b) multi-storey frame structure

Considering the single-storey case study, a precast concrete building with plan dimensions 87.5x76.3 m is selected. The columns, 7.65 m high, are connected to the foundation through grouted sleeves and placed at the corners of a 17.5 x 10.9 m net. The columns support inverted T and L pre-stressed beams in the short direction, supporting double-T pre-stressed roof elements spanning in the other direction. **Figure 7a** and **Figure 7b** represent the double-T roof-to-beam and the beam-to-column connections, respectively: the former is constituted by arch-shape ductile connections, reported in Belleri et al. [15], placed at each double-T stem, while the latter is constituted by two grouted sleeves with 28 mm diameter bolts, 640 MPa yield stress and 800 MPa ultimate stress, anchored in the column top. The arch-shape device increases the rotational stiffness of the beam-to-beam connection and provides energy dissipation. Being the roof elements designed as pin-supported structures for gravity loads, their geometry is known from the gravity loads design, leading to known values of the bending moment capacity of the connections, herein taken as 210 kNm for the beam-to-column connection and 210 kNm for the sum of the bending moment capacities of the double-T to beam connections present in the column tributary area. It is worth noting that the bending moment capacity associated to each arch-shape device (**Figure 7a**) has been evaluated as the product between the axial capacity of the arch shape device and the distance between such device and the centre of the topping. The seismic mass corresponding to a single column tributary area is 86’700 kg.

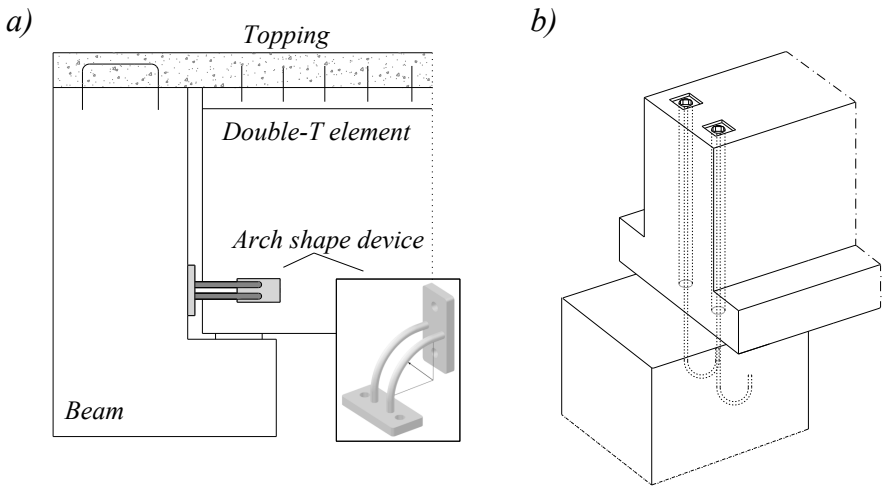

Figure 7 – a) double-T to beam connection; b) beam-to-column connection

The DBD procedure is applied to the selected case study; a target inter-storey drift of 2.5% is chosen for demonstration purpose representing damage control [38, 39]. The inter-storey drift is defined as the ratio between relative storey displacement and inter-storey height. For comparison sake the DBD procedure is applied to the same case study with pinned beam-to-column connections. **Table 3** reports the results of the DBD procedure and the NLTH analyses; the latter expressed in terms of mean, maximum and standard deviation of the set of values constituted by the maximum drift obtained for each ground motion. The finite element model scheme is shown in **Figure 6a**; the properties of elements and connections are reported in Appendix D. The results in **Table 3** show a general good agreement between the target and the obtained drift values in terms of mean values. In the case of not-emulative beam-to-column connections, the effective height is lower and the displacement ductility is higher; in addition, more conservative results are obtained. This is related to the computation of the equivalent viscous damping based on global ductility; in fact at a local ductility level the connections experience a higher ductility demand and therefore a higher contribution in viscous damping. It is worth noting that in the hinged-frame case, which directly resembles a SDOF system, the DBD target is well reflected by the mean results of NLTH analyses. This is a direct consequence of the calibration of the equivalent viscous damping (step 7 of the procedure presented in chapter 3), based on mean values in the present paper; a calibration of the equivalent viscous damping based on a lower percentile would lead to more conservative results. The choice of such percentile is a topic of ongoing research.

Table 3 – DBD and NLTH analyses results for the single-storey case study: hinged and not-emulative frame

DBD – hinged frame						
Iteration	H_{eff} **(m)**	μ_D	V_{base} **(kN)**	M_{col} **(kNm)**	α_2	T_{eff} **(s)**
1	7.65	2.12	173	1321	0	1.99
2	7.65	2.12	173	1318	0	1.95
Column 70x70 cm – 16 26mm diam. rebars – M_u = 1334 kNm – T = 0.97s						
NLTH analyses results (in terms of drift)						
DBD target		**NLTH mean**		**NLTH max**		**NLTH std**
2.50 %		2.44 %		4.38%		1.15 %
DBD – not-emulative frame (M_y^{con} = 210 kNm)						
Iteration	H_{eff} **(m)**	μ_D	V_{base} **(kN)**	M_{col} **(kNm)**	α_2	T_{eff} **(s)**
1	5.60	2.54	224	939	0.197	1.43
2	5.49	2.59	222	894	0.207	1.43
3	5.41	2.62	222	885	0.209	1.41
4	5.40	2.63	222	882	0.210	1.41
Column 65x65 cm – 16 22mm diam. rebars – M_u = 952 kNm – T = 1.03s						
NLTH results (in terms of drift)						
DBD target		**NLTH mean**		**NLTH max**		**NLTH std**
2.50 %		2.10 %		3.76%		0.92 %

Considering the multi-storey case, a 3-storey precast concrete building with plan dimensions 24x24 m is selected. The columns are continuous along the building height and connected to the foundation through grouted sleeves. The inter-storey height is 4 m and the bay length is 6 m in both directions. The floors are constituted by inverted T and L pre-stressed beams and double-T pre-stressed elements. The three static schemes of **Figure 5** are considered. For demonstration purposes, only the plane constituted by the inverted T and L beams is analysed. The seismic mass is 400 kg/m^2 and 800 kg/m^2 for intermediate and roof level respectively. The DBD procedure is applied to the selected case study considering a design drift of 2.5%. The procedure results are reported in **Table 4** as a function of the considered static scheme.

Table 4 – DBD results: multi-storey case study.
Note: OTM stands for overturning moment

Iteration	H_{eff} (m)	μ_D	V_{base} (kN)	M_{col} (kNm)	α_3	T_{eff} (s)
Case A (Figure 5a)						
1	9.13	1.34	172	1578	0	1.31
2	9.13	1.32	175	1598	0	1.30
3	9.13	1.32	175	1598	0	1.30
Column 80x80 cm – 16 26mm diam. rebars – M_u = 1600 kNm – T = 0.55s						
Case B (Figure 5b – M_y^{con} = 125 kNm)						
1	9.13	1.24	184	1442	0.065	1.26
2	9.09	1.35	168	1284	0.073	1.34
3	9.09	1.36	166	1266	0.074	1.35
4	9.09	1.37	166	1264	0.074	1.35
Column 75x75 cm – 16 24mm diam. rebars – M_u = 1296 kNm – T = 0.62s OTM taken by change of axial load in the column (Figure 5) is 16% of total OTM						
Case C (Figure 5c – M_y^{con} = 125 kNm)						
1	9.13	0.93	243	1747	0.107	1.10
2	9.07	1.06	202	1363	0.137	1.24
3	9.04	1.12	189	1240	0.151	1.29
4	9.03	1.15	183	1188	0.159	1.31
5	9.03	1.16	181	1162	0.161	1.33
6	9.02	1.17	179	1149	0.163	1.33
7	9.02	1.18	179	1142	0.164	1.34
8	9.02	1.18	178	1137	0.165	1.34
9	9.02	1.18	178	1135	0.165	1.34
Column 60x60 cm – 16 26mm diam. rebars – M_u = 1146 kNm – T = 0.67s OTM taken by change of axial load in the column (Figure 5) is 29% of total OTM						

Figure 6b shows the finite element model scheme, whose properties are reported in Appendix D. **Table 5** reports the results of the NLTH analyses for all the considered static schemes, expressed in terms of mean, maximum and standard deviation of the set of values constituted by the maximum inter-storey drift obtained for each ground motion. **Figure 8** provides a graphic representation of the results in terms of mean drift and mean deflected shape compared to the DBD predictions. A general good agreement between the target and the obtained values is observed, particularly for Case A and Case B. Case C, which is characterized by the lowest scatter of the results, presents a slight underestimation both in terms of drift and deflected shape. This is related to the computation of the equivalent viscous damping based on global ductility, as in the case of single-storey frames. Beside this, the presented conservative formulation is herein suggested for the considered structural typology. Further research is required to highlight the influence of various connections configuration in the equivalent viscous damping formulation.

Table 5 – NLTH analyses results (inter-storey drift): multi-storey case study

Static scheme	Floor	DBD result (%)	NLTH mean (%)	NLTH max (%)	NLTH std (%)
Case A (Figure 5a)	1	0.87	1.24	2.65	0.71
	2	2.04	2.08	3.54	0.76
	3	2.50	2.54	3.92	0.77
Case B (Figure 5b)	1	0.94	1.14	2.37	0.64
	2	2.12	2.10	3.32	0.77
	3	2.50	2.53	3.70	0.75
Case C (Figure 5c)	1	1.05	0.89	1.23	0.18
	2	2.26	1.82	2.60	0.41
	3	2.50	2.17	3.13	0.45

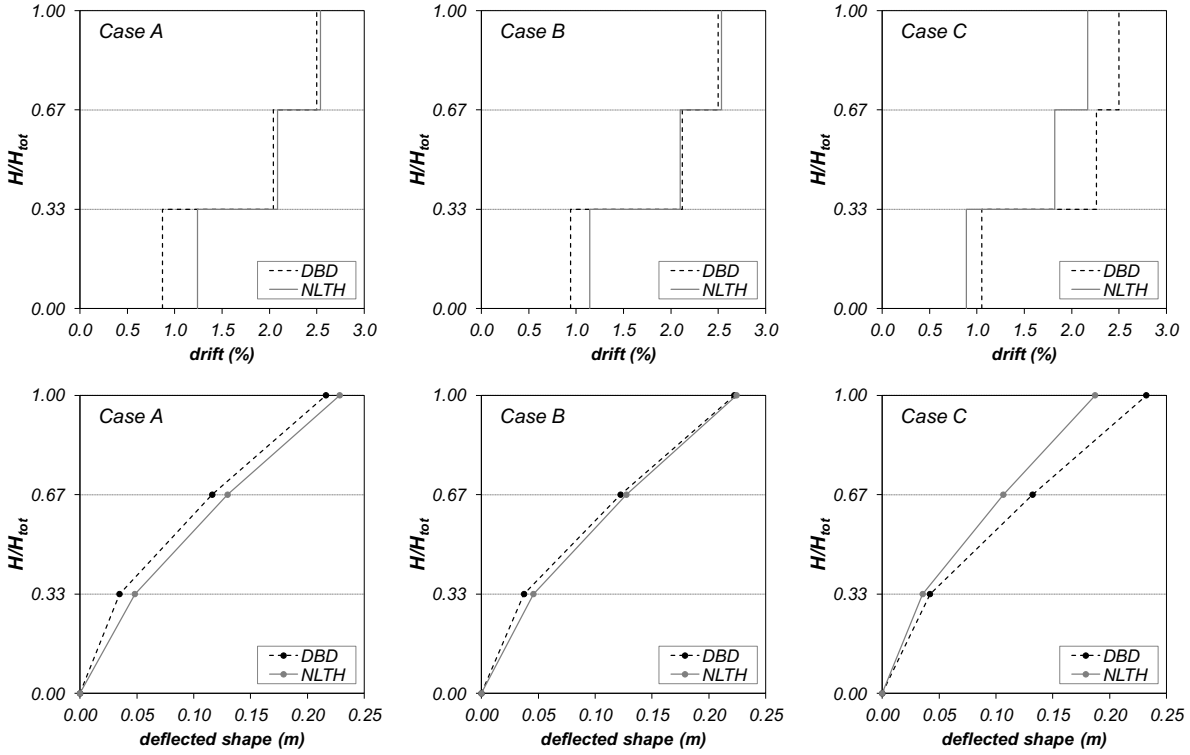

Figure 8 – Comparison between DBD predictions and NLTH analyses results in terms of mean values of drift (top row) and deflected shape (bottom row)

To estimate the safety of the designed buildings, pushover analyses have been conducted in accordance to EN 1998-1 [24]. The results are expressed in terms of the ratio between the collapse and design peak ground acceleration (PGA); such ratios are 1.43, 1.39, 1.47, 1.63, 1.71 for the single-storey hinged frame, not-emulative frame and multi-storey Case A, B and C, respectively. The pushover analysis considered the failure of the plastic hinge at the column base. It is observed that beam-to-column connections contribute to increase the PGA associated to structural failure in the multi-storey case, provided that such connections have been detailed to accommodate the required rotation demand. The opposite happens in the single-storey case. In general, the difference in the PGA ratios could partially be related to the displacement ductility demand: the lower the

displacement ductility demand the higher the collapse PGA. Finally, it is worth noting that the same DBD approach could be used also to design the structure at the collapse prevention limit state. In the case of emulative connections, the general procedure developed by Priestley et al. [26] for reinforced concrete frames could be adopted.

Conclusions

The Displacement Based Design (DBD) procedure was herein adapted for the application to precast concrete frames typical of the European practice. New expressions for the DBD were developed considering peculiar aspects of precast structures as column-to-foundation and beam-to-column connections for both single-storey and multi-storey buildings. In particular, regarding column-to-foundation connections, a new formula was proposed for the yield curvature estimation; such formulation is able to capture for instance the difference between the cross-section depth and the effective depth typical of some precast connections, as in the case of grouted sleeves. A novel algorithm was developed to calibrate the hysteretic damping expression associated to different types of connections, allowing for a faster solution by means of inelastic spectra.

Regarding beam-to-column connections, the effects of a degree of fixity was eventually considered for both single-storey and multi-storey structures. New expressions were derived for the target displacement and displacement ductility in single-storey frames. Refined yield displacement formulas were derived for multi-storey frames; such formulas are also suitable for shear wall and coupled shear wall structures.

The proposed procedure was validated by means of non-linear time history analyses considering single-storey and multi-storey buildings with hinged or not-emulative connections. A general good agreement between the DBD target values and the obtained results was observed. The highest scatter of the results was associated to hinged frames. Not-emulative connections generally provided more conservative results both in terms of drift and deflected shape. This is related to the computation of the equivalent viscous damping based on global ductility; in fact, at a local ductility level the connections experience a higher ductility demand and therefore a higher contribution in viscous damping. Beside this, the presented conservative formulation is herein suggested for the considered structural typology. Further research is required to highlight the influence of various connections configuration in the equivalent viscous damping formulation.

It is worth noting that eventually the results are affected by the choice made in the definition of the percentile used in the equivalent viscous damping calibration. In the present paper the calibration was based on average results; a calibration based on a lower percentile would lead to more conservative results. The choice of such percentile is a topic of ongoing research.

Acknowledgements

The author gratefully acknowledges the financial support of the Italian RELUIS project and the careful review and constructive suggestions by the anonymous reviewers.

References

[1] Park R (1995) “A Perspective on the seismic design of precast concrete structures in New Zealand”, PCI Journal, 40(3):40-60

[2] Restrepo JI, Park R, Buchanan AH, (1995) "Design of Connections of Earthquake Resisting Precast Reinforced Concrete Perimeter Frames", PCI Journal, 40(5):68-80

[3] Priestley MJN, Sritharan S, Conley JR, Pampanin S (1999) "Preliminary Results and Conclusions from the PRESSS Five-Story Precast Concrete Test-Building", PCI Journal, 44(6):42–67

[4] Englekirk RE (1995), Development and testing of a ductile connector for assembling precast concrete beams and columns, PCI Journal, 40(2):36-51

[5] Pampanin S, Park R (2005) "Appendix B: Special provisions for the seismic design of jointed ductile precast concrete connections", In NZS3101: 2005, Concrete Structures Standard

[6] Schoettler MJ, Belleri A, Zhang D, Restrepo JI, Fleishman RB, (2009) "Preliminary results of the shake-table testing for the development of a diaphragm seismic design methodology", PCI Journal, 54(1):100-124

[7] Belleri A, Schoettler MJ, Restrepo JI, Fleischman RB, (2014) "Dynamic behavior of rocking and hybrid cantilever walls in a precast concrete building", ACI Structural Journal, 111(3):661-672.

[8] Metelli G, Beschi C, Riva P (2011) "Cyclic behaviour of a column to foundation joint for concrete precast structures", European Journal of Environmental and Civil Engineering, 15(9):1297-1318

[9] Belleri A, Riva P (2012) "Seismic performance and retrofit of precast grouted sleeve connections", PCI Journal, 57(1):97-109

[10] Dal Lago B, Toniolo G, Lamperti M (2016) "Influence of different mechanical column-foundation connection devices on the seismic behaviour of precast structures", Bulletin of Earthquake Engineering, 14(12):3485–3508

[11] Tullini N, Minghini F (2016) "Grouted sleeve connections used in precast reinforced concrete construction – Experimental investigation of a column-to-column joint", Engineering Structures, 127:784-803

[12] Psycharis IN, Mouzakis HP (2012) "Assessment of the seismic design of precast frames with pinned connections from shaking table tests", Bulletin of Earthquake Engineering, 10(6):1795–1817

[13] Zoubek B, Fahjan J, Isakovic T, Fischinger M (2013) "Cyclic failure analysis of the beam-to-column dowel connections in precast industrial buildings engineering structures", Engineering Structures, 52:179–191

[14] Magliulo G, Ercolino M, Cimmino M, Capozzi V, Manfredi G (2014) "FEM analysis of the strength of RC beam-to-column dowel connections under monotonic actions", Construction and Building Materials, 69:271–284

[15] Belleri A, Torquati M, Riva P (2014) "Seismic performance of ductile connections between precast beams and roof elements", Magazine of Concrete Research, 66(11):553-562

[16] Belleri A, Torquati M, Marini A, Riva P (2016) "Horizontal cladding panels: in-plane seismic performance in precast concrete buildings", Bulletin of Earthquake Engineering, DOI: 10.1007/s10518-015-9861-8

[17] Belleri A, Brunesi E, Nascimbene R, Pagani M, Riva P (2014) "Seismic Performance of Precast Industrial Facilities Following Major Earthquakes in the Italian Territory", J. Perform. Constr. Facil., doi:10.1061/(ASCE)CF.1943-5509.0000617

[18] Belleri A, Torquati M, Riva P, Nascimbene R (2015) "Vulnerability assessment and retrofit solutions of precast industrial structures", Earthquake and Structures. 8(3): 801-820

[19] Belleri A, Torquati M, Marini A, Riva P (2015) “In-plane seismic performance of horizontal cladding panels in industrial precast concrete buildings” Submitted for possible publication to Bulletin of Earthquake Engineering

[20] Fischinger M, Zoubek B, Isakovic T (2014) Seismic response of precast industrial buildings. Perspectives on European Earthquake Engineering and Seismology: Vol. 1. Ansal A (editor), Springer, Berlin, pp 131-177

[21] Zoubek B, Fischinger M, Isaković T, (2016) “Cyclic response of hammer-head strap cladding-to-structure connections used in RC precast building”, Engineering Structures, 119:135-148

[22] Magliulo G, Ercolino M, Petrone C, Coppola O, Manfredi G (2014) “The Emilia Earthquake: Seismic Performance of Precast Reinforced Concrete Buildings”, Earthquake Spectra, 30(2):891-912

[23] Scotta R, De Stefani L, Vitaliani R, (2015) “Passive control of precast building response using cladding panels as dissipative shear walls”, Bulletin of Earthquake Engineering, 13(11):3527-3552

[24] CEN (2004), EN 1998-1:2004, Eurocode 8: Design of structures for earthquake resistance - Part 1: General rules, seismic actions and rules for buildings, European Committee for Standardization, Brussels, Belgium.

[25] Biondini F, Toniolo G, Tsionis G (2010) “Capacity design and seismic performance of multi-storey precast structures”, European Journal of Environmental and Civil Engineering, 14(1): 11-28

[26] Priestley MJN, Calvi GM, Kowalsky MJ (2007) “Displacement-Based Seismic Design of Structures”, IUSS Press, Pavia, Italy

[27] Shibata A, Sozen M, (1976) “Substitute structure method for seismic design in reinforced concrete”, ASCE Journal of Structural Engineering, 102(1):1-18

[28] Dwairi HM, Kowalsky MJ, Nau JM (2007) “Equivalent Damping in Support of Direct Displacement-Based Design”, Journal of Earthquake Engineering, 11:512-530

[29] Grant DN, Blandon CA, Priestley MJN, (2004) “Modelling Inelastic Response in Direct Displacement-Based Design”, IUSS Press Pavia, Italia.

[30] Otani S, (1974) “SAKE: A Computer Program for Inelastic Response of R/C Frames to Earthquakes”, Civil Engineering Studies SRS-413, University of Illinois at Urbana-Champaign, 11/1974

[31] Pennucci D, Sullivan TJ, Calvi GM (2011) “Displacement Reduction Factors for the Design of Medium and Long Period Structures”, Journal of Earthquake Engineering, 15(S1):1-29

[32] Montejo LA, Kowalsky MJ (2007) “CUMBIA – Sets of codes for the analysis of reinforced concrete members”, North Carolina State University, Raleigh, NC, USA

[33] Carr AJ (2006), Ruaumoko, Users manuals, University of Canterbury, Christchurch, New Zealand

[34] Marriott D, Pampanin S, Bull D, Palermo A (2008) “Dynamic Testing of Precast, Post-Tensioned Rocking Walls Systems with Alternative Dissipating Solutions”, Bulletin of the New Zealand Society for Earthquake Engineering, 41(2):90-103

[35] Pennucci D, Calvi GM, Sullivan TJ (2009) “Displacement-Based Design of Precast Walls with Additional Dampers”, Journal of Earthquake Engineering, 13(1):40-65

[36] MidasGEN (2012) v3.1, MIDAS Information Technologies Co. Ltd

[37] Ambraseys N, Smit P, Douglas J et al. (2004) Internet-site for European strong-motion data. Bollettino di Geofisica Teorica ed Applicata 45(3): 113–129

555 [38] Calvi GM, Sullivan TJ (2009) "A Model Code for the Displacement-Based Seismic Design of
556 Structures", IUSS Press, Pavia, Italy

557 [39] FEMA 450, (2004) "NEHRP recommended provisions for seismic regulations for new buildings and
558 other structures", Building seismic safety council, national institute of building sciences, Washington DC

559

APPENDIX A: Derivation of Eqn. 17 and 18

Considering the moment distribution of **Figure 4** with a bending moment $2M_y^{con}$ and M_y^{col} at the column tip and base respectively, H_{eff} is:

$$H_{eff} = \frac{H}{M_y^{col} + 2M_y^{con}} M_y^{col} = \frac{H}{1+2\alpha_2} \tag{A.1}$$

where $\alpha_2 = M_y^{con} / M_y^{col}$.

The yield displacement at the inflection point is:

$$\Delta_y^{IP} = \frac{\phi_y^{col} H_{eff}^{\ 2}}{3} = \frac{\phi_y^{col} H^2}{3} \frac{1}{(1+2\alpha_2)^2} \tag{A.2}$$

The displacement at the inflection point associated to the rotation of the plastic hinge at the column base is:

$$\Delta_{plast}^{IP} = \Delta_{plast}^{roof} \frac{H_{eff}}{H} = \frac{\Delta_{plast}^{roof}}{1+2\alpha_2} = \frac{1}{1+2\alpha_2}\left[\beta H - \phi_y^{col} \frac{H^2}{3}(1-\alpha_2)\right] \tag{A.3}$$

Therefore Eqn. 17 is obtained:

$$\begin{aligned} \Delta_d^{IP} &= \Delta_y^{IP} + \Delta_{plast}^{IP} = \frac{\phi_y^{col} H^2}{3} \frac{1}{(1+2\alpha_2)^2} + \frac{1}{1+2\alpha_2}\left[\beta H - \phi_y^{col} \frac{H^2}{3}(1-\alpha_2)\right] = \\ &= \frac{\phi_y^{col} H^2}{3} \frac{\alpha_2(2\alpha_2 - 1)}{(1+2\alpha_2)^2} + \frac{\beta H}{1+2\alpha_2} \end{aligned} \tag{A.4}$$

Eqn. 18 is obtained directly as:

$$\mu_\Delta = \frac{\Delta_d^{IP}}{\Delta_y^{IP}} = \frac{\dfrac{\phi_y^{col} H^2}{3} \dfrac{\alpha_2(2\alpha_2 - 1)}{(1+2\alpha_2)^2} + \dfrac{\beta H}{1+2\alpha_2}}{\dfrac{\phi_y^{col} H^2}{3} \dfrac{1}{(1+2\alpha_2)^2}} = \alpha_2(2\alpha_2 - 1) + \frac{3\beta(1+2\alpha_2)}{\phi_y^{col} H} \tag{A.5}$$

APPENDIX B: Derivation of Eqn. 21

Considering the triangular distribution of lateral forces according to **Figure B.1a**, the bending moment associated to the ith floor is:

$$M_i = F \sum_{h=1}^{n-p} (n-h+1)\left(H_{n-h+1} - H_i\right) \tag{B.1}$$

Substituting $H_i = i \cdot \Delta H$ and $H_n = n \cdot \Delta H$ where ΔH is the inter-storey height:

$$\begin{aligned} M_i &= F \cdot \Delta H \sum_{h=1}^{n-p} (n-h+1)(n-h+1-i) = \\ &= F \cdot \Delta H \sum_{h=1}^{n-p} \left[n^2 + 2n - n \cdot i + 1 - i + h^2 + h(-2n - 2 + i)\right] \end{aligned} \tag{B.2}$$

From the fundamental properties of series

$$\sum_{z=1}^{m}(z) = \frac{m(m+1)}{2}; \quad \sum_{z=1}^{m}(z^2) = \frac{2m^3 + 3m^2 + m}{6} \tag{B.3; B.4}$$

the following expression of M_i is obtained:

$$M_i = F\cdot\Delta H\left[\begin{array}{l}(n-i)\left(n^2+2n-n\cdot i+1-i\right)+\dfrac{2(n-i)^3+3(n-i)^2+(n-i)}{6}+\\ +(-2n+i-2)\dfrac{(n-i)(n-i+1)}{2}\end{array}\right]= \tag{B.5}$$

$$=\frac{F\cdot\Delta H}{6}\left[i^3-i(3n^2+3n+1)+n(2n^2+3n+1)\right]$$

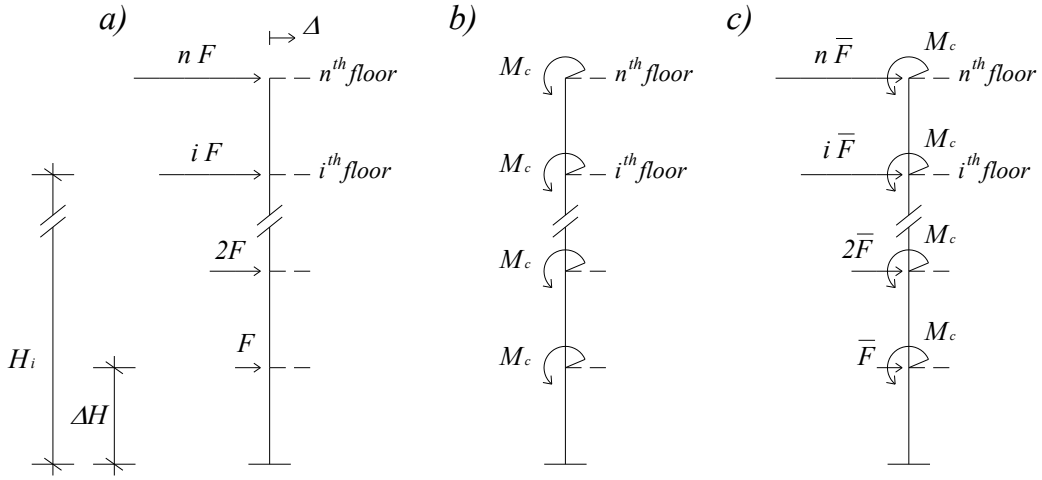

Figure B.1 – Static scheme considered for lateral deflection evaluation.

Substituting $i = H_i/\Delta H$, $\Delta H = H_n/n$ and $n\cdot\Delta H = H_n$:

$$M_i = \frac{F}{6}\left[\frac{H_i^3}{H_n^2}n^2 - H_i(3n^2+3n+1)+H_n(2n^2+3n+1)\right] \tag{B.6}$$

Considering the base moment (H_i=0):

$$M_b = \frac{F}{6}H_n(2n^2+3n+1) \tag{B.7}$$

From which F is obtained:

$$F = \frac{6M_b}{H_n(2n^2+3n+1)} \tag{B.8}$$

Substituting back in Eqn. A2.6:

$$M_i = \frac{M_b}{2n^2+3n+1}\left[\left(\frac{H_i}{H_n}\right)^3 n^2 - \frac{H_i}{H_n}(3n^2+3n+1)+(2n^2+3n+1)\right] \tag{B.9}$$

Considering the curvature along the column height, $\phi_i = M_i/EI$, the column rotation (θ_i) and lateral displacement (Δ_i) at the ith floor are respectively:

$$\theta_i = \frac{M_b}{(2n^2+3n+1)EI}\left[\frac{1}{4}\frac{H_i^4}{H_n^3}n^2 - \frac{1}{2}\frac{H_i^2}{H_n}(3n^2+3n+1)+H_i(2n^2+3n+1)+A\right] \tag{B.10}$$

$$\Delta_i = \frac{M_b}{(2n^2+3n+1)EI}\left[\frac{1}{20}\frac{H_i^5}{H_n^3}n^2 - \frac{1}{6}\frac{H_i^3}{H_n}(3n^2+3n+1)+\frac{H_i^2}{2}(2n^2+3n+1)+AH_i+B\right] \tag{B.11}$$

Where A and B (integration's constants) are both equal to 0 being $\theta_i = 0$ and $\Delta_i = 0$ at the base (i.e. H_i=0). Eqn. 21 is obtained considering yielding at the column base (i.e. $M_b/EI = \phi_y$):

601 $$\Delta_{y,i}^{hinged} = \frac{\phi_y}{2n^2+3n+1}\left[\frac{H_i^5}{20\cdot H_n^3}n^2 - \frac{H_i^3}{6\cdot H_n}\left(3n^2+3n+1\right)+\frac{H_i^2}{2}\left(2n^2+3n+1\right)\right] \quad \text{(B.12)}$$

602 APPENDIX C: Derivation of Eqn. 22

603 To derive Eqn. 22 it is first necessary to consider the deflected shape associated to yielding of all
604 column-to-beam connections (**Figure B.1b**). The bending moment distribution on the column is
605 stepped, with a value at the i[th] floor equal to:

606 $$M_i = (n-i+1)M_c \quad \text{(C.1)}$$

607 The deflected shape is obtained by double integration of the column curvature:

608 $$\begin{aligned}
\Delta_i &= -\sum_{h=1}^{i}\frac{M_h}{EI}\left(H_h - H_{h-1}\right)\left[\frac{H_h - H_{h-1}}{2}+\left(H_i - H_h\right)\right] = \\
&= -\sum_{h=1}^{i}(n-h+1)\frac{M_c}{EI}\left(H_h - H_{h-1}\right)\left[\frac{H_h - H_{h-1}}{2}+\left(H_i - H_h\right)\right] = \\
&= -\sum_{h=1}^{i}(n-h+1)\frac{M_c}{EI}\Delta H\left[\frac{\Delta H}{2}+\Delta H\left(i-h\right)\right] = \\
&= -\frac{M_c}{EI}\frac{\Delta H^2}{2}\sum_{h=1}^{i}(n-h+1)\left(2i-2h+1\right) = \\
&= -\frac{M_c}{EI}\frac{\Delta H^2}{2}\left[-\frac{i^3}{3}+i^2\left(n+\frac{1}{2}\right)-\frac{1}{6}i\right]
\end{aligned} \quad \text{(C.2)}$$

609 Substituting $i = H_i/\Delta H$ and $\Delta H = H_n/n$:

610 $$\Delta_i = -\frac{M_c}{2EI}H_i\left[-\frac{1}{3}n\frac{H_i^2}{H_n}+H_i\left(n+\frac{1}{2}\right)-\frac{1}{6}\frac{H_n}{n}\right] \quad \text{(C.3)}$$

611 The rotation at the i[th] floor is:

612 $$\theta_i = -\frac{M_c}{2EI}\left[-n\frac{H_i^2}{H_n}+2H_i\left(n+\frac{1}{2}\right)-\frac{1}{6}\frac{H_n}{n}\right] \quad \text{(C.4)}$$

613 Considering the static scheme depicted in **Figure B.1c**, the lateral force required to obtain the same
614 base moment as in **Figure B.1a** is:

615 $$\overline{F}_i = F_i + n\frac{M_c H_i}{\sum_{j=1}^{n}H_j^2} \quad \text{(C.5)}$$

616 Following the same procedure adopted to derive Eqn. 21, the lateral displacement associated to such
617 lateral force distribution is:

618 $$\begin{aligned}
\Delta_{y,i} &= \left(1+n\frac{M_c}{M_b}\right)\frac{\phi_y}{2n^2+3n+1}\left[\frac{H_i^5}{20\cdot H_n^3}n^2 - \frac{H_i^3}{6\cdot H_n}\left(3n^2+3n+1\right)+\frac{H_i^2}{2}\left(2n^2+3n+1\right)\right] = \\
&= \left(1+n\frac{M_c}{M_b}\right)\Delta_{y,i}^{hinged}
\end{aligned} \quad \text{(C.6)}$$

619 Finally, the total lateral displacement is obtained adding Eqn. A3.3 to Eqn. A3.6:

620 $$\Delta_{y,i}^{connection} = \Delta_{y,i}^{hinged}\left(1+n\cdot\frac{M_c}{M_b}\right)-\frac{1}{2}\frac{M_c}{M_b}\frac{M_b}{EI}\left[-\frac{n\cdot H_i^3}{3\cdot H_n}+\left(n+\frac{1}{2}\right)H_i^2-\frac{H_i\cdot H_n}{6\cdot n}\right] \quad \text{(C.7)}$$

621 The corresponding rotation is

$$\theta_{y,i}^{connection} = \theta_{y,i}^{hinged}\left(1+n\cdot\frac{M_c}{M_b}\right)-\frac{1}{2}\cdot\frac{M_c}{M_b}\cdot\frac{M_b}{EI}\left[-n\frac{H_i^2}{H_n}+2H_i\left(n+\frac{1}{2}\right)-\frac{1}{6}\frac{H_n}{n}\right] \quad \text{(C.8)}$$

APPENDIX D: Properties of finite element models

Considering the finite element models, the beam-to-column connection has been modelled with the same Takeda hysteresis used for the column-to-foundation connection (r = 0.005, $\alpha = 0.35$ and $\beta = 0$ – **Figure 2**) for both single-storey and multi-storey structures, owing the demonstrative purpose of the present study. **Table D.1** contains the parameters used in the finite element models.

Table D.1 – finite element model properties

Common data					
Concrete	Strength f_c = 40 MPa; elastic modulus E_c = 35'000 MPa				
Steel	Strength f_y = 450 MPa; elastic modulus E_s = 210'000 MPa				
Beam	Inverted-T, Area A = 0.595 m^2, Second moment of area I = 0.04674m^4				
Beam-to-column connection	stiffness k_{con} = 200'000 kNm/rad				
Takeda hysteresis	r = 0.005, α = 0.35 and β = 0				
Specific data					
	Single-storey Hinged frame	Single-storey Connections	Multi-storey Case A	Multi-storey Case B	Multi-storey Case C
Static scheme	**Figure 6a**	**Figure 6a**	**Figure 5a**	**Figure 5b**	**Figure 5c**
Column cross-section	70x70cm	65x65cm	80x80cm	75x75cm	60x60cm
Nodal mass (kg)	86'700	86'700	28'800 (1st - 2nd storey); 14'400 (3rd storey)		
M_y^{col} (kNm)	1334	952	1600	1296	1146
M_y^{con} (kNm)	0	210	0	125	125